13th International Symposium on Turbulence and Shear Flow Phenomena (TSFP13)
Montreal, Canada, June 25–28, 2024

WALL-MODELED LARGE-EDDY SIMULATIONS OF WALL HEATING AND COOLING EFFECTS IN SHOCK-TURBULENT BOUNDARY LAYER INTERACTIONS

Vanessa Rubien
Department of Aerospace and Mechanical Engineering
University of Southern California
Los Angeles, CA 90089, USA
vrubien@usc.edu

Ivan Bermejo-Moreno
Department of Aerospace and Mechanical Engineering
University of Southern California
Los Angeles, CA 90089, USA
bermejom@usc.edu

ABSTRACT

Wall-modeled large-eddy simulations (WMLES) of supersonic turbulent boundary layers with and without shock-wave interactions and wall heat transfer are conducted, and the results are compared against reference experimental and DNS data. The main objective is to evaluate the performance of equilibrium wall models to accurately capture complex patterns of boundary layer separation. Separated shock/turbulent-boundary-layer interactions (STBLI) and no-shock turbulent boundary layer cases are simulated with a freestream Mach number of approximately 2.3 and momentum-thickness Reynolds numbers of 2.5×10^3 and 4.1×10^3 over cooled, adiabatic, and heated walls. Results show that WMLES exhibit a qualitative agreement with DNS data in patterns of flow separation induced by strong STBLIs with wall heat transfer, whereby wall heating/cooling enlarges/reduces the extent of separated flow. The quantitative accuracy is significantly affected by the choice of WMLES parameters. In particular, a reduction of the wall-model exchange height in the STBLI region improves significantly the prediction of friction and heat-flux coefficients. The influence of the subgrid-scale (SGS) model parameter and the wall-model turbulent Prandtl number is also assessed for the flow without shock waves.

INTRODUCTION

At the high speeds encountered by supersonic and hypersonic vehicles, the compressibility of air flow leads to the formation of shock waves that can interact with the turbulent boundary layers developed over internal or external surfaces. Viscous heating at high speeds produces elevated near-wall temperatures, leading to coupling between fluid flow, heat transfer, and, possibly, structural mechanics. This coupling can have significant aerodynamic and thermostructural consequences that impact the performance of high-speed systems, ranging from increased drag due to boundary layer separation to structural deformation or failure due to excessive thermal loading. As such, there is significant motivation to accurately predict these aero-thermal-structural interactions, especially at lower financial and computational costs.

STBLI behavior has been studied extensively, but most experimental studies (Schreyer *et al.*, 2018; Combs *et al.*, 2019; Lu *et al.*, 2020) and numerical studies (Priebe & Martín, 2012; Pasquariello *et al.*, 2017; Zuo *et al.*, 2019) in this area have been limited to adiabatic wall conditions. However, surfaces exposed to the flow in high-speed systems are generally not adiabatic, and heat transfer to the vehicle is an important design consideration. Previous research has shown that wall heating and cooling alter the flow physics of turbulent boundary layers and can have an even greater impact when shock waves are present. In a previous computational study, wall temperature changes below an oblique STBLI showed that wall heating and cooling increase and decrease the size of the separated-flow region, respectively (Bernardini *et al.*, 2016).

Physical experiments have historically served as the gold standard for data in high-speed flow-structure-interaction (FSI) analysis. Experimental studies have explored the effects of wall heat transfer on supersonic turbulent boundary layers and STBLIs (Debieve *et al.*, 1997; Jaunet *et al.*, 2014; Schülein, 2006), but near-wall experimental measurements can be challenging. In recent decades, direct numerical simulation (DNS) and wall-resolved large-eddy simulation (LES) have been shown to predict STBLIs with a high level of accuracy, bridging some of the gaps in experimental data (Pirozzoli & Bernardini, 2011). DNS and LES, however, incur extremely high computational costs in order to resolve near-wall scales and capture the low-frequency motion of shocks and separation that are relevant, for example, to the potential coupling with the structure. WMLES is intended to mitigate excessive computational cost by coarsening the LES grid near the wall while modeling a portion of the turbulent boundary layer (Larsson *et al.*, 2016). This allows for longer time integration over larger and more complex geometries, making WMLES a desirable method for studying the low-frequency motions and multi-dimensional aero-thermal-structural dynamics present in STBLI.

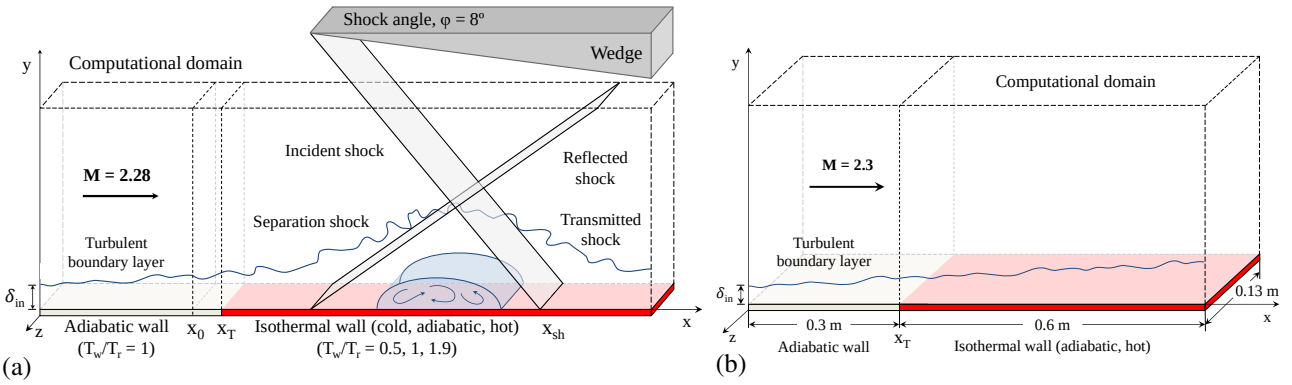

Figure 1. Schematic of the (a) STBLI case flow configuration based on Bernardini *et al.* (2016) DNS study and (b) no-shock TBL case flow configuration based on Debieve *et al.* (1997) experimental study.

The objectives of this research are to a) investigate the effects of wall heat flux on STBLI and turbulent boundary layers in high-speed flows and b) assess the accuracy and parameter sensitivity of WMLES in comparison to experimental and DNS methods. To this end, two cases will be explored: an STBLI case with wall heating and cooling and a simple turbulent boundary layer case (without a shock) with wall heating. The second case will be used to analyze how specific wall-model parameters affect the development of a turbulent boundary layer subjected to wall heating.

COMPUTATIONAL SETUP

Case configurations

Figure 1(a) shows a schematic of the STBLI case flow configuration based on the reference DNS study of Bernardini *et al.* (2016). The size of the computational flow domain is $111.5\delta_{\text{in}} \times 11.7\delta_{\text{in}} \times 5.5\delta_{\text{in}}$ in the streamwise (x), wall-normal (y), and spanwise directions (z), where δ_{in} is defined as the inflow boundary layer thickness. The grid spacing is $(\Delta x/\delta_0, \Delta z/\delta_0) \approx (0.08, 0.05)$ and $\Delta y/\delta_0$ varies from a uniform value of 0.0125 below and at the wall model exchange height to 0.05 at the boundary layer edge, further stretched geometrically above, where $\delta_0 = 1.45\delta_{\text{in}}$ is the boundary layer thickness at the reference location, $x_0 = 50\delta_{\text{in}}$. The wall-normal grid spacing is uniform from the wall up to the exchange location, then varies according to a hyperbolic tangent up to the reference boundary layer thickness, followed by geometric stretching up to the upper boundary. This translates to a mesh size of $N_x \times N_y \times N_z = 960 \times 131 \times 76$, producing a mesh consisting of approximately 9.5 million total cells. An oblique shock wave impinges on an incoming turbulent boundary layer developed over a flat plate in a Mach 2.28 air flow. This interaction produces the region of interest, characterized by the interaction length scale, L, defined as the distance between the foot of the separation shock and the estimated inviscid incident shock impingement point, $x_{\text{sh}} = 69.5\delta_{\text{in}}$. The turbulent boundary layer first develops over adiabatic wall conditions by imposing a wall temperature equal to the recovery temperature ($T_w = T_r$) up to a streamwise location, x_T, where a gradual wall temperature variation is imposed in the region $54.5\delta_{\text{in}} < x < 58.5\delta_{\text{in}}$ following:

$$T_w(x) = T_r\left[1 + \frac{s-1}{2}\left(1 + \tanh\frac{2(x-(x_T+2.5))}{\delta_{\text{in}}}\right)\right] \quad (1)$$

The value of x_T in equation 1 is shifted 2.5 units downstream from the x_T in Bernardini *et al.* (2016) in order to more accurately position the temperature step change within the transition region. Downstream of the wall temperature transition region, local heating or cooling is applied for the remainder of the domain ($x > x_T$) based on a wall-to-recovery temperature ratio, $s = T_w/T_r$. The wall conditions investigated include cooled ($s = 0.5$), adiabatic ($s = 1.0$), and heated ($s = 1.9$) walls.

Figure 1(b) shows the schematic of the no-shock TBL case flow configuration based on experiments conducted by Debieve *et al.* (1997). In this experiment, a turbulent boundary layer develops over a flat plate in Mach 2.3 air flow without a shock wave. Similar to the previous case, the turbulent boundary layer develops over adiabatic wall conditions up to the wall temperature change location, x_T, then wall heating is applied for the remainder of the domain ($x > x_T$). The wall temperatures investigated in this configuration include adiabatic ($s = 1.0$) and heated ($s = 1.5, 2.0$) walls.

Numerical methodology

The flow solver in the present simulations is a 2$^{\text{nd}}$-order finite-volume shock-capturing compressible large-eddy simulation that integrates the spatially-filtered compressible Navier-Stokes equations on body-fitted, unstructured meshes (Hoy & Bermejo-Moreno, 2022). A solution-adaptive blend of a low-dissipative, centered numerical scheme in shock-free, turbulent flow regions and an essentially non-oscillatory scheme near shock waves is employed, using a shock sensor inspired by Ducros *et al.* (1999). The explicit subgrid-scale model proposed by Vreman (2004) is used to resolve smaller turbulent eddies near the wall. Time integration is executed using explicit 4$^{\text{th}}$-order Runge-Kutta time stepping. At the inflow, synthetically generated turbulence using a digital filtering technique (Klein *et al.*, 2003; Xie & Castro, 2008) is introduced with imposed mean and fluctuating velocity wall-normal profiles extracted from Pirozzoli & Bernardini (2011) at a Mach number of 2 and Re_τ of 200, adequately rescaled to provide $M_\infty \approx 2.28$, $\delta_0/\delta_{in} \approx 1.45$, and $Re_\tau \approx 450$ at the reference streamwise location, x_0. Rankine-Hugoniot relations are imposed at the top boundary of the computational domain to generate the incident oblique shock.

On the bottom, the equilibrium wall model of Kawai & Larsson (2012) is employed, in which the inner part ($y < h_{\text{wm}}$) of the turbulent boundary layer is modeled, where h_{wm} is the wall-model exchange height. Equilibrium conditions are assumed in the inner region of the boundary layer, resulting in the following ODE system, simplified from the momentum

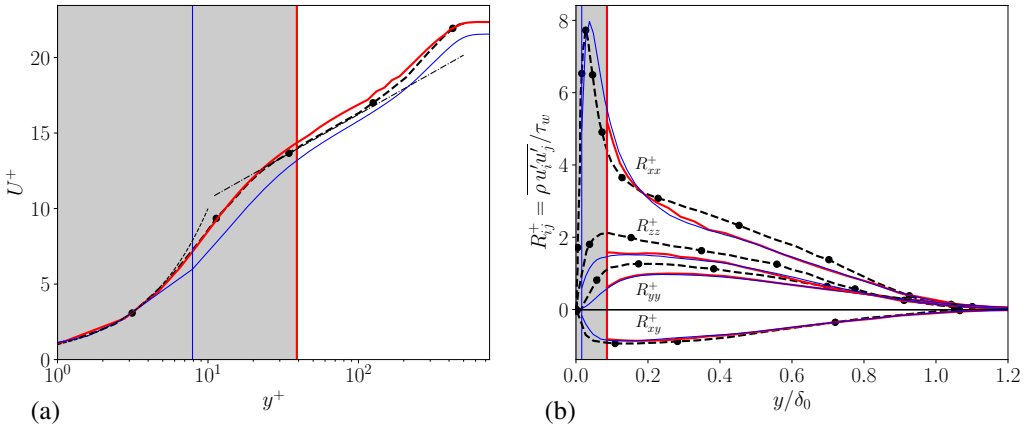

Figure 2. Wall-normal profiles of (a) van Driest-transformed mean streamwise velocity and (b) density-scaled Reynolds stress components of the incoming turbulent boundary layer of the STBLI case, extracted at the reference location ($x_0 = 50\delta_{\text{in}}$), comparing present WMLES results (solid) with DNS data (dashed, with symbols) from Bernardini *et al.* (2016). Red lines correspond to WMLES with $h_{\text{wm}} = 0.1\delta_0$, whereas blue lines correspond to WMLES with the exchange location placed at the first wall-adjacent grid cell. The wall-modeled region is indicated with a gray background and a vertical line of the corresponding color. Dotted and dashed-dotted black lines represent theoretical approximations of mean streamwise profiles in the viscous sublayer (y^+) and log-law region ($\ln(y^+)/0.41 + 5.0$).

and total energy conservation equations (Larsson *et al.*, 2016):

$$\frac{\mathrm{d}}{\mathrm{d}y}\left[(\mu + \mu_{t,\text{wm}})\frac{\mathrm{d}U}{\mathrm{d}y}\right] = 0 \quad (2)$$

$$\frac{\mathrm{d}}{\mathrm{d}y}\left[c_p\left(\frac{\mu}{Pr} + \frac{\mu_{t,\text{wm}}}{Pr_{t,\text{wm}}}\right)\frac{\mathrm{d}T}{\mathrm{d}y} + (\mu + \mu_{t,\text{wm}})U\frac{\mathrm{d}U}{\mathrm{d}y}\right] = 0 \quad (3)$$

where U and T are the wall-parallel velocity and temperature, respectively. c_p is the specific heat capacity at constant pressure. Pr is the fluid Prandtl number, representing the momentum-to-thermal fluid diffusivity ratio, and $Pr_{t,\text{wm}}$ is the turbulent Prandtl number in the wall model, representing the eddy diffusivity ratio. μ is the dynamic viscosity of the fluid and $\mu_{t,\text{wm}}$ is the eddy viscosity defined as $\mu_{t,\text{wm}} = \kappa\rho\sqrt{\tau_w/\rho}y[1-\exp(-y^+/A^+)]^2$, with constants $\kappa = 0.41$, $A^+ = 17$, and $Pr_{t,\text{wm}} = 0.9$. The + superscripts indicate variables expressed in inner wall units, scaled by the viscous length, $\ell_v = \mu_w/(\rho_w u_\tau)$, where $u_\tau = \sqrt{\tau_w/\rho_w}$, and w subscripts denote wall quantities. Other scaling approaches, such as semilocal and mixedmin2 scaling, have shown improved predictions in cold-wall flows and could be considered in future work (Iyer & Malik, 2019).

The wall-model height determines the location between the wall-model grid and LES grid where information is exchanged. In particular, this is where the LES grid provides the wall-model with the velocity, pressure, and temperature values required to solve the wall-model ODE system, which then returns values of wall shear stress and heat flux to be used by the LES grid. The wall model height is typically chosen around 10-20% of the boundary layer thickness, several grid cells above the wall, to reduce numerical errors in the exchanged variables from the LES (Kawai & Larsson, 2012). For compressible flows over diabatic walls, the effect of the exchange height in the accuracy of wall-model predictions is less understood, and recent studies have found significant sensitivity in a priori analyses (Iyer & Malik, 2019). Adequately accounting for near-wall heat transfer effects by using an exchange location closer to the wall could dominate over the larger expected numerical errors. In this study, we conduct simulations first with a uniform wall-model height equal to 10% of the boundary layer thickness at the reference location ($h_{\text{wm}} = 0.1\delta_0$), and, second, with a variable wall-model height that decreases near the STBL interaction region from $0.1\delta_0$ to the centroid of the first cell adjacent to the wall, while maintaining the same background LES grid.

RESULTS

Incoming boundary layer

Figure 2a shows van Driest-transformed mean streamwise velocity profiles in inner units at a reference streamwise location in the adiabatic region upstream of the interaction, $x_0 = 50\delta_{\text{in}}$, comparing DNS reference data and two WMLES with different wall-model exchange heights, h_{wm}: one simulation sets h_{wm} at 10% of the reference boundary layer thickness (corresponding to the fourth grid cell from the wall), whereas the other WMLES sets the exchange location of the wall model at the first wall-adjacent cell centroid. The vertical colored lines indicate the exchange location, and the gray shading indicates the wall-modeled region for wall-normal distances below the exchange height ($y \leq h_{\text{wm}}$). Above the wall-modeled region ($y > h_{\text{wm}}$), the data corresponds to the LES solution, such that for each WMLES, the wall-model and LES wall-normal are combined into a single line. WMLES data using a standard wall-model exchange height of 10% of the reference boundary layer thickness shows a close agreement with the reference DNS data in the viscous, buffer and part of the wake regions, with a slight overprediction in part of the log-law layer above $y^+ \approx 20$ (red line). Agreement is restored again in the wake region. The friction Reynolds number at that reference station closely matches the DNS value of $Re_\tau \approx 450$. This relatively low Re_τ translates into a short log-law region. Results for the simulation using the same LES grid but lowering the wall-model exchange height to the location of the centroid of the first cell adjacent to the wall are shown in blue. Due to the low Re_τ, that brings the exchange location to the lower end of the buffer sublayer, and results in an underprediction of the van Driest transformed mean velocity profile throughout most of the boundary layer.

Figure 2(b) shows wall-normal profiles of density-scaled Reynolds stresses above the wall-model exchange height ($y \geq h_{\text{wm}}$) at the reference streamwise location in outer units. In contrast to the mean streamwise velocity profile, the wall

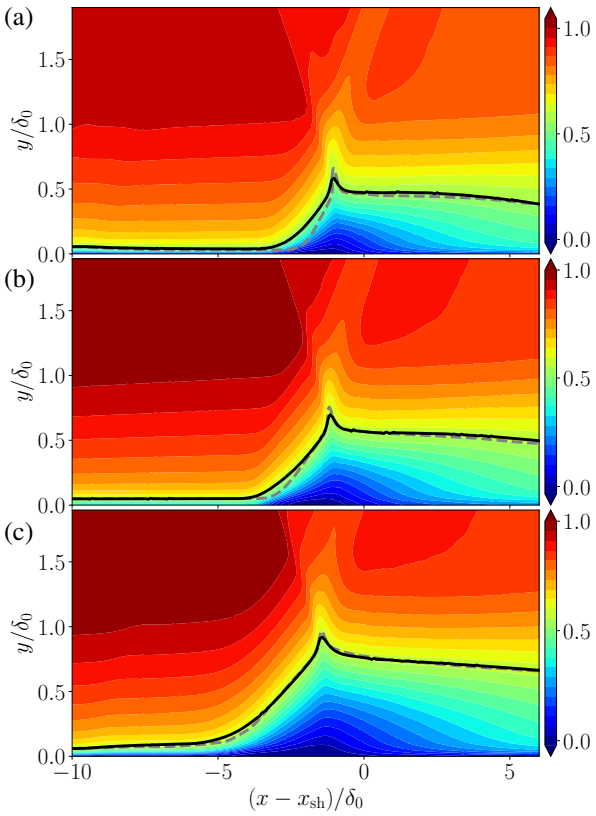

Figure 3. STBLI case contours of normalized time- and spanwise averaged streamwise velocity, $\overline{u}/u_\infty$, on a vertical plane obtained from WMLES with variable h_{wm} for cases with (a) cooled, (b) adiabatic, and (c) heated bottom walls. The solid black and dashed gray lines indicate the averaged sonic line ($M = 1$) from current WMLES simulations and DNS by Bernardini *et al.* (2016), respectively.

model does not provide Reynolds stresses to combine with the plotted LES solution. The Reynolds stresses obtained from the LES solution below the wall model exchange height ($y \leq h_{\text{wm}}$) are expected to be more affected by numerical errors (Kawai & Larsson, 2012), and are omitted. The Reynolds stress components in this figure reflect results from the standard 10% wall-model exchange height simulation (in red) and from the first wall-adjacent cell centroid (in blue). The prediction of these velocity fluctuations by the LES appears mostly unaffected by the choice of wall-model exchange height considered in these simulations, compared with the larger impact observed on the van Driest-transformed mean streamwise velocity. The Reynolds shear stress, $\widetilde{u'v'}$, produced by the WMLES shows especially close agreement with reference DNS data. Although the wall-normal ($\widetilde{v'v'}$) and spanwise ($\widetilde{w'w'}$) Reynolds stresses are slightly underpredicted, the WMLES results show sufficient overall agreement with reference data to indicate that the incoming turbulent boundary layer upstream of the interaction with the shock is being modeled with reasonable accuracy when the exchange height of the wall model is placed at 10% of the reference boundary layer thickness.

Interaction region

Figure 3 shows contour plots of time- and spanwise-averaged streamwise velocity in the interaction region, highlighting prominent flow features present in STBLI and the impact of wall temperature on the extent of the interaction. As the boundary layer interacts with the shock system, turbulence is amplified and the boundary layer thickens. Shock-induced mean flow separation is observed in all cases, highlighted by dark blue regions. Compared to the adiabatic case, the size of the separation bubble increases with wall heating and decreases with wall cooling, qualitatively following the DNS results. The sonic line moves toward the wall with wall cooling and away from the wall with wall heating, owing to the combined effects of a density increase near the wall (to maintain an approximately constant pressure across the boundary layer) and the reduced separation bubble resulting from wall cooling, which allows the shock to impinge deeper into the turbulent boundary layer. As a result, higher near-wall speeds can be reached with wall cooling. A quantitative comparison between the averaged sonic lines obtained from the WMLES and the reference DNS data shows an overall good agreement throughout most of the interaction region, with the exception of the zone near the separation shock, where the subsonic part of the boundary layer appears thicker than in the DNS (more so for lower wall temperatures). This discrepancy might be due to more stringent grid resolution requirements for strong wall cooling cases.

Wall quantities (skin friction and heat flux)

The streamwise profiles of skin friction coefficient for the STBLI cases are shown in Figure 4, presenting qualitatively similar features for all wall temperatures under consideration. In the cooled and heated cases, there is a local maximum and minimum, respectively, at the wall temperature transition location, $(x_T - x_{\text{sh}})/\delta_0 \approx -9$. This is followed by a global minimum for all wall temperatures where the skin friction coefficient becomes negative in the interaction region, indicating an area of separated flow. This negative region spans a larger distance for the heated case and a smaller distance for the cooled case, confirming that the size of the separation bubble increases with increasing wall temperature, as anticipated by the contours of mean streamwise velocity in Figure 3, and consistent with the DNS reference data.

When WMLES simulations are run at a standard 10% wall-model height, mean separation is absent and the local extrema of the skin friction coefficient occurring at the wall temperature transition location are also not well-captured. However, the skin friction coefficient upstream and downstream of the interaction is more accurately predicted. Lowering h_{wm} to coincide with the first cell-centroid adjacent to the wall (while keeping the same resolution) translates into the WMLES better predicting the skin friction coefficient at and near the interaction region, showing better agreement with DNS data. In particular, the skin friction variations along the temperature transition and separation bubble are captured much more accurately, both qualitatively and quantitatively. The cooled wall case shows a slight overprediction compared to the adiabatic and heated wall cases. Despite the generally improved agreement in the interaction region, WMLES with the lowered wall-model exchange height exhibit worsened prediction of the skin friction in the recovery region downstream.

The impact of a lower wall model height can also be seen in the wall heat flux. Figure 5 illustrates the behavior of heat transfer at the wall for cooled and heated wall conditions. The predictions obtained with a standard wall model height of $h_{\text{wm}} = 0.1\delta_0$ in the present simulations appear to miss qualitative trends within the interaction region. For simulations with a lowered wall-model exchange height, the expected trends are captured, by which an increase in magnitude of the wall heat transfer along the interaction region is observed, followed by

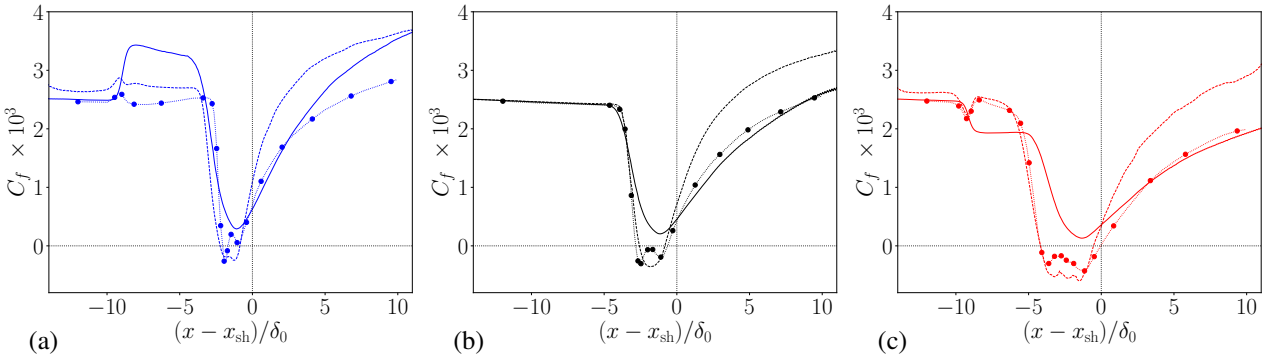

Figure 4. Streamwise distribution of skin friction coefficient, C_f, for STBLI cases with (a) cooled, (b) adiabatic, and (c) heated bottom wall temperatures. Dotted lines with symbols indicate reference DNS data from Bernardini *et al.* (2016), solid lines indicate WMLES results at a constant wall-model height (10% of the reference boundary layer thickness), and dashed lines indicate WMLES results with the wall-model exchange height set to the first wall-adjacent cell centroid.

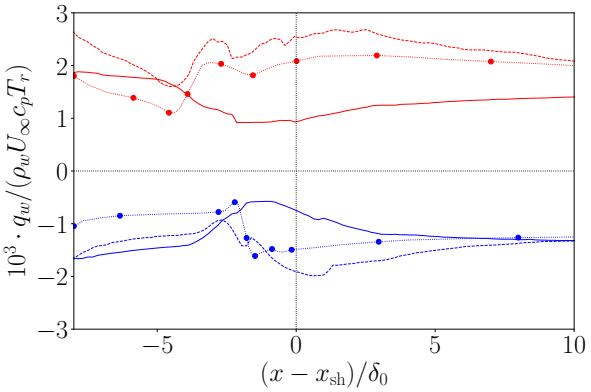

Figure 5. Streamwise distribution of wall heat flux, q_w, for STBLI cases with cooled (blue) and heated (red) bottom wall temperatures. Dotted lines with symbols indicate reference DNS data from Bernardini *et al.* (2016), solid lines indicate WMLES results at a constant wall-model height (10% of the reference boundary layer thickness), and dashed lines indicate WMLES results with the wall-model exchange height set to the first wall-adjacent cell centroid.

relaxation to a new equilibrium. Despite recovering these qualitative trends, the present WMLES results lack quantitative accuracy for heat flux predictions, relative to the DNS data.

Model parametric studies

In light of the challenges associated with quantitative agreement of WMLES predictions of skin friction and heat flux distributions for heated and, especially, cooled walls, the purpose of the second case configuration (TBL with no shock), replicating experiments by Debieve *et al.* (1997), is to gain additional insight into the prediction of these wall quantities in the absence of shock interaction using WMLES. For this configuration, we conduct parametric studies varying the constant coefficient of Vreman's subgrid-scale model (c) and the wall-model turbulent Prandtl number ($Pr_{t,\mathrm{wm}}$).

Variation of the Vreman coefficient, a subgrid scale model parameter, primarily impacts the resulting skin friction coefficient. Looking at both $s = 1.5$ and $s = 2.0$ cases, Figure 6(a) illustrates how lowering the subgrid-scale Vreman coefficient from its nominal $c = 0.07$ value to 0.03 causes a decrease in the skin friction coefficient, whereas Figure 6(b) shows a much lesser effect of this parameter on the heat transfer coefficient, calculated as $C_h = q_w/(\rho_\infty U_\infty c_p(T_r - T_w))$, where c_p is the specific heat capacity at constant pressure, and the subscript ∞ denotes freestream variables. For the $s = 1.5$ heated case, we observe in Figure 6(b) a large dependency of the heat transfer coefficient on the wall-model turbulent Prandtl number. Increasing $Pr_{t,\mathrm{wm}}$ also produces a notable increase in the skin friction coefficient, as seen in Figure 6(a).

CONCLUSIONS

In this study, the effects of wall heating and cooling on supersonic boundary layers with and without shock interactions are investigated using wall-modeled large-eddy simulations (WMLES). WMLES is found capable of accurately capturing mean streamwise velocity profiles and Reynolds stress data over the adiabatic portion of the wall, with a standard wall-model height of 10% of the boundary layer thickness. Consistent with DNS results, shock-induced flow separation increased with wall heating and decreased with wall cooling. Separated flow in the interaction region, however, was only accurately predicted for the present WMLES when the exchange height was locally reduced upstream and throughout that interaction region, while keeping the same LES background grid. This reduction in the h_{wm} also improved skin friction predictions in the region of temperature transition located upstream of the interaction of the boundary layer with the shock, but worsened the predictive accuracy in the recovery region.

The use of a variable wall-model exchange height also translated into significantly better predictions of wall heat transfer over cooled and heated walls by the WMLES, although still showing quantitative differences with DNS. The ad-hoc approach of varying the wall-model exchange height from a standard 10% boundary layer thickness value over most of the adiabatic wall upstream of the STBLI region and decreasing it in diabatic wall regions could be replaced in practical settings with sensor-based approaches that adapt the wall-model height accordingly.

The effects of Vreman's subgrid-scale coefficient and the wall-model turbulent Prandtl number on the skin friction and heat transfer predictions was also evaluated, finding a significant impact in the predictions, compared with experimental data. Overall, the ability to accurately model STBLI over nonadiabatic surfaces at a more practical computational cost is a critical and viable step in the pursuit of modern high-speed aerodynamics technology.

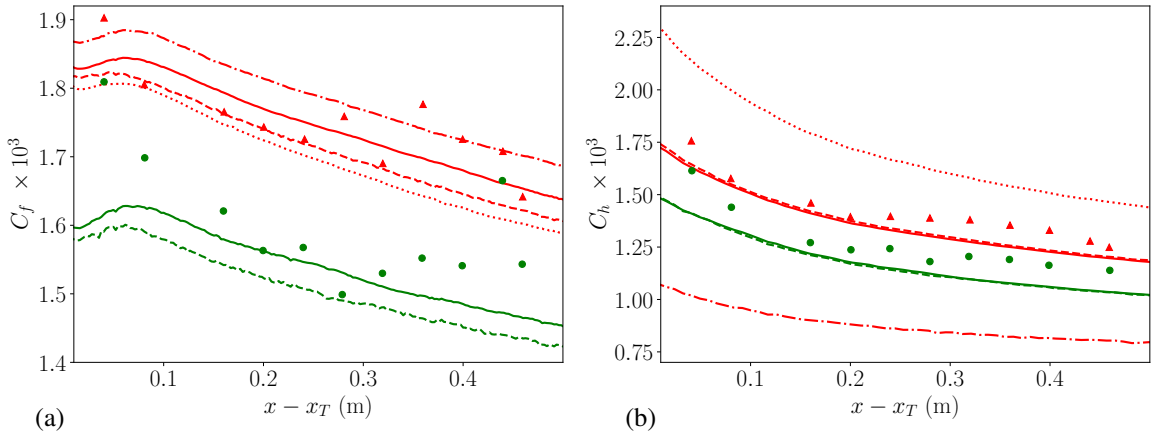

Figure 6. Streamwise distributions of (a) skin friction coefficient, C_f, and (b) heat transfer coefficient, C_h, obtained from present WMLES (lines) in comparison with reference data from experiments by Debieve *et al.* (1997) (symbols) of a supersonic turbulent boundary layer subject to step change wall heating with $s = 1.5$ (red lines and triangles) and $s = 2$ (green lines and circles). Solid lines correspond to WMLES using the nominal values of Vreman's SGS model coefficient ($c = 0.07$) and turbulent Prandtl number ($Pr_t = 0.9$). Dashed lines use a reduced Vreman SGS coefficient of $c = 0.03$, keeping $Pr_t = 0.9$. The dash-dotted line corresponds to $Pr_t = 2$ and the dotted line to $Pr_t = 0.5$, with $c = 0.07$ and $s = 1.5$ in both cases.

ACKNOWLEDGMENT

This work was supported by the National Defense Science and Engineering Graduate Fellowship, the National Science Foundation (grant 2143014), and an Early Career Faculty grant from NASA's Space Technology Research Grants Program (grant 80NSSC23K1497). Computational resources were provided by the Center for Advanced Research Computing at the University of Southern California.

REFERENCES

Bernardini, M., Asproulias, I., Larsson, J., Pirozzoli, S. & Grasso, F. 2016 Heat transfer and wall temperature effects in shock wave turbulent boundary layer interactions. *Phys. Rev. Fluids* **1** (8), 084403.

Combs, C. S., Schmisseur, J. D., Bathel, B. F. & Jones, S. B. 2019 Unsteady analysis of shock-wave/boundary-layer interaction experiments at mach 4.2. *AIAA J.* **57** (11), 4715–4724.

Debieve, J.-F., Dupont, P., Smith, D. R. & Smits, A. J. 1997 Supersonic turbulent boundary layer subjected to step changes in wall temperature. *AIAA J.* **35** (1), 51–57.

Ducros, F., Ferrand, V., Nicoud, F., Weber, C., Darracq, D., Gacherieu, C. & Poinsot, T. 1999 Large-eddy simulation of the shock/turbulence interaction. *J. Comput. Phys.* **152** (2), 517–549.

Hoy, J. & Bermejo-Moreno, I. 2022 Fluid–structural coupling of an impinging shock–turbulent boundary layer interaction at Mach 3 over a flexible panel. *Flow* **2**, E35.

Iyer, P. S. & Malik, M. R. 2019 Analysis of the equilibrium wall model for high-speed turbulent flows. *Phys. Rev. Fluids* **4** (7), 074604.

Jaunet, V., Debiève, J. & Dupont, P. 2014 Length scales and time scales of a heated shock-wave/boundary-layer interaction. *AIAA J.* **52** (11), 2524–2532.

Kawai, S. & Larsson, J. 2012 Wall-modeling in large eddy simulation: Length scales, grid resolution, and accuracy. *Phys. Fluids* **24** (1).

Klein, M., Sadiki, A. & Janicka, J. 2003 A digital filter based generation of inflow data for spatially developing direct numerical or large eddy simulations. *J. Comput. Phys.* **186** (2), 652–665.

Larsson, J., Kawai, S., Bodart, J. & Bermejo-Moreno, I. 2016 Large eddy simulation with modeled wall-stress: recent progress and future directions. *Mech. Eng. Rev.* **3** (1), 15–00418.

Lu, X., Yi, S., He, L., Liu, X. & Zhang, F. 2020 Experimental study on time evolution of shock wave and turbulent boundary layer interactions. *J. Appl. Fluid Mech.* **13** (6), 1769–1780.

Pasquariello, V., Hickel, S. & Adams, N. A. 2017 Unsteady effects of strong shock-wave/boundary-layer interaction at high reynolds number. *J. Fluid Mech.* **823**, 617–657.

Pirozzoli, S. & Bernardini, M. 2011 Direct numerical simulation database for impinging shock wave/turbulent boundary-layer interaction. *AIAA J.* **49** (6), 1307–1312.

Priebe, S. & Martín, M. P. 2012 Low-frequency unsteadiness in shock wave–turbulent boundary layer interaction. *J. Fluid Mech.* **699**, 1–49.

Schreyer, A.-M., Sahoo, D., Williams, O. J. & Smits, A. J. 2018 Experimental investigation of two hypersonic shock/turbulent boundary-layer interactions. *AIAA J.* **56** (12), 4830–4844.

Schülein, E. 2006 Skin friction and heat flux measurements in shock/boundary layer interaction flows. *AIAA J.* **44** (8), 1732–1741.

Vreman, A. 2004 An eddy-viscosity subgrid-scale model for turbulent shear flow: Algebraic theory and applications. *Phys. Fluids* **16** (10), 3670–3681.

Xie, Z.-T. & Castro, I. 2008 Efficient generation of inflow conditions for large eddy simulation of street-scale flows. *Flow Turbul. Combust.* **81**, 449–470.

Zuo, F.-Y., Memmolo, A., Huang, G.-p. & Pirozzoli, S. 2019 Direct numerical simulation of conical shock wave–turbulent boundary layer interaction. *J. Fluid Mech.* **877**, 167–195.